Bioorganic Chemistry 114 (2021) 105038

Contents lists available at ScienceDirect

Bioorganic Chemistry

journal homepage: www.elsevier.com/locate/bioorg

Synthesis of new hydrazone derivatives and evaluation of their monoamine oxidase inhibitory activity

Fatih Tok [a], Begüm Nurpelin Sağlık [b,c], Yusuf Özkay [b,c], Sinem Ilgın [d], Zafer Asım Kaplancıklı [b], Bedia Koçyiğit-Kaymakçıoğlu [a,*]

[a] Department of Pharmaceutical Chemistry, Faculty of Pharmacy, Marmara University, Istanbul, Turkey
[b] Department of Pharmaceutical Chemistry, Faculty of Pharmacy, Anadolu University, Eskişehir, Turkey
[c] Doping and Narcotic Compounds Analysis Laboratory, Faculty of Pharmacy, Anadolu University, Eskişehir, Turkey
[d] Department of Pharmaceutical Toxicology, Faculty of Pharmacy, Anadolu University, Eskişehir, Turkey

ARTICLE INFO

Keywords:
Hydrazone
Urea
MAO
Docking
ADME

ABSTRACT

A novel series of hydrazone derivatives were designed and synthesized. Their structures were characterized by IR, ^{1}H NMR, ^{13}C NMR and HR-MS spectroscopic methods. The newly synthesized compounds were evaluated for their inhibitory activity against monoamine oxidase enzymes (MAO-A and MAO-B). Compounds **2a**, **2k**, **4a** and **4i** showed significant inhibitory activity against MAO-A, with IC_{50} value in the range of 0.084–0.207 μM compared to reference drug moclobemide (IC_{50} value = 6.061 μM). These compounds (**2a**, **2k**, **4a** and **4i**) were exposed to cytotoxicity tests to establish their preliminary toxicological profiles and were found to be non-cytotoxic. Moreover, the most effective compound **4i** was evaluated using enzyme kinetics and docking studies to elucidate the plausible mechanisms of inhibition of MAO-A. According to enzyme kinetic studies, compound **4i** was a reversible and competitive inhibitor with similar inhibition features as the substrates. Also, it was seen that this compound was settled down very properly at the active site of MAO-A enzyme by doing important interactions owing to the docking studies. Finally, ADME predictions were applied to estimate pharmacokinetic profiles of synthesized compounds. According to calculated ADME predictions, all parameters of the compounds were within the standard ranges in terms of "Rule of Five" and "Rule of Three" and it was detected that the synthesized compounds (**2a**-**4i**) have good and promising pharmacokinetic profiles.

1. Introduction

Monoamine oxidase catalyzes the oxidative deamination of biogenic and xenobiotic amines and it has two isoforms MAO-A and MAO-B [1]. Differences between MAO-A and MAO-B include aminoacid sequences, sensitivity to inhibitors, substrate specificity and intensity of tissue [2]. MAO-A is generally indicated in catecholaminergic neurons of the cortex while MAO-B is found in serotonergic neurons, in the brain [3]. MAO-A inhibitors are mostly used in the treatment of depression, whereas MAO-B inhibitors are mainly used in the treatment of Parkinson's and Alzheimer's. MAO-A inhibitors also are useful in the treatment of neuropsychiatric disorders, including anxiety, autism and attention deficit hyperactivity disorder [4]. MAO inhibitors are also identified as neuroprotective agents because they can decrease the amount of hydrogen peroxide and aldehyde species that lead to neuronal cell damage [5].

The first-generation irreversible MAO inhibitors were used as antidepressant drugs but non-selective or irreversible MAO inhibitors caused serious side-effects such as tachycardia, hepatotoxicity, drug and food interactions such as serotonin syndrome, tyramine-induced hypertensive crisis (cheese-effect) (tyramine reaction) [6–8]. However, MAO inhibitors were proposed as second choice agents after serotonin reuptake inhibitors by the American Psychiatric Association [9]. Although current MAO inhibitors are known to be useful for neurodegenerative disorders such as Alzheimer's, Parkinson's diseases, or Depression, these drugs are not enough to fight against these diseases and many of them have only symptomatic effects [10]. Therefore, considering all these features, involvement of deregulated metabolism of monoamines in neurodegenerative and neuropsychiatric diseases [11], the design and development of more effective and more selective drug candidates are needed for the discovery of useful therapeutic agents.

Hydrazones consist of a reaction between a carbonyl compound

* Corresponding author at: Department of Pharmaceutical Chemistry, Faculty of Pharmacy, Marmara University, 34854 4/A Istanbul, Turkey.
E-mail address: bkaymakcioglu@marmara.edu.tr (B. Koçyiğit-Kaymakçıoğlu).

https://doi.org/10.1016/j.bioorg.2021.105038
Received 6 April 2021; Received in revised form 10 May 2021; Accepted 28 May 2021
Available online 1 June 2021

(aldehyde or ketone) and a hydrazine molecule by the elimination of water [12]. Hydrazone derivatives, containing the —C═N—NH— group, plays an important role in discovering new drug molecules [13]. They exhibit a broad spectrum of biological activities, such as antimicrobial, antidepressant, anticonvulsant, anti-inflammatory, anticancer. Hydrazones bear two different connected nitrogen atoms and these structural cores are generally responsible for the physical and chemical properties [14]. The carbon atom of hydrazone shows both electrophilic and nucleophilic character [15]. Therefore hydrazones are used widely in the design of new molecules having a variety of activities.

The identification of the crystal structures of the two isoforms of human MAO and the selective interactions between the enzymes and their ligands allows the determination of the pharmacophoric groups required for the rational design of new inhibitors. It is reported that the substrates and inhibitors of MAOs usually bear imino or amino groups that can interact with the active site of the enzyme easily [16,17]. In addition to hydrazone derivatives, urea and amide moiety have long been known for their important monoamine oxidase inhibitory activity [18–21]. In this study, we designed and synthesized a new hydrazone bearing urea/amide moiety. We investigated their inhibitory activity against MAO-A and MAO-B enzymes. Some electron-withdrawing and electron donor groups on the aromatic ring in this synthesis were used to find out the effects of the substituents on monoamine oxidase inhibitory activity.

2. Results and discussion

2.1. Chemistry

The general pathway of synthesis was given in Fig. 1. Firstly, *4-aminoacetophenone* is treated with different isocyanate in dichloromethane and different benzoyl chloride in chloroform to get the corresponding urea and amide derivatives, respectively. Then condensation reaction takes place between 2,4-dinitrophenyl hydrazine and starting material on the ketone group in methanol to get target molecules.

All new hydrazone derivatives were confirmed by IR, ^{1}H NMR, ^{13}C NMR and HR-MS spectroscopic methods. In the ^{1}H NMR spectra of compounds, N—H stretching vibrations appeared at 3296–3404 cm^{-1}. The strong sharp absorption bands at 1645–1680 cm^{-1} were attributed to C═O stretching vibrations of amide and urea moieties. Also, characteristic bands at 1602–1649 cm^{-1} were assigned to C═N stretching vibrations. In the ^{1}H NMR spectra of the compounds, N—H protons belonging to hydrazone and amide moieties resonated at 11.08–11.13 ppm, 10.28–10.98 ppm respectively. However, N—H protons belonging to urea moieties appeared with aromatic protons. Protons of the —CH$_3$ group were observed at 2.35–2.45 ppm as singlets. Aromatic and other aliphatic protons were detected in the estimated regions. In the ^{13}C NMR spectra of the compounds, C═O carbons of amide or urea moieties were recorded at 162.47–166.28 ppm. The C═N carbons of the hydrazone group gave a signal at 153.08–154.61 ppm. In the HR-MS spectra of the compounds, all masses were in accordance with the expected M + H and M−H values.

2.2. In vitro MAO-A and MAO-B inhibition

The *in vitro* fluorometric method declared previously by our research group [22–26] was used to evaluate the inhibition potency of the synthesized compounds on MAO isoforms. Table 1 represents the first step of enzyme activity assay; while, Fig. 2 points out the second step. In the second step, the reference inhibitors and selected compounds that showed more than 50% inhibitory activity at 10^{-4} M concentration were prepared in their further concentrations by serial dilutions (ranging from 10^{-5} M to 10^{-9} M). Therefore, the half maximal inhibitory concentration (IC_{50}) values of the selected compounds and reference inhibitors could be calculated and these results are given in Fig. 2.

In summary, it was understood from Table 1 that some compounds in the series displayed remarkable inhibition potency at 10^{-3} M concentration; however, none of them showed significant inhibitory activity at 10^{-4} M concentration on MAO-B enzyme. Generally it was claimed that all synthesized compounds showed selective MAO-A enzyme inhibitory activity. It was observed that compounds **2a**, **2k**, **4a** and **4i** performed seriously effective inhibition profile at 10^{-4} M concentration against MAO-A enzyme and thus, these compounds were included in the second stage of enzyme activity assay. Compound **4i** was found to be the most effective agent in the series with the IC_{50} value of 0.084 ± 0.003 μM. Furthermore, it was noteworthy that this compound performed an inhibition profile 72 times more effective than reference drug moclobemide (IC_{50} value = 6.061 ± 0.262 μM). Besides, compounds **2a**, **2k** and **4a** were identified as the other most active derivatives in the series with the IC_{50} values of 0.207 ± 0.010 μM, 0.187 ± 0.008 μM and 0.138 ± 0.005 μM, respectively.

2.3. Enzyme kinetics

Enzyme kinetics studies help to determine the type of inhibition of the compound on the enzyme and also identify the inhibition as irreversible or reversible. The linear Lineweaver-Burk graphs are the most common method for this. For this purpose, compound **4i** was included in the enzyme kinetic assay to evaluate the inhibition type on MAO-A enzyme. Enzyme kinetic assay was applied in the same way as previously mentioned [22–26]. The IC_{50}/2, IC_{50}, and 2(IC_{50}) were used as the concentrations of compound **4i**. The velocity curves of the substrates

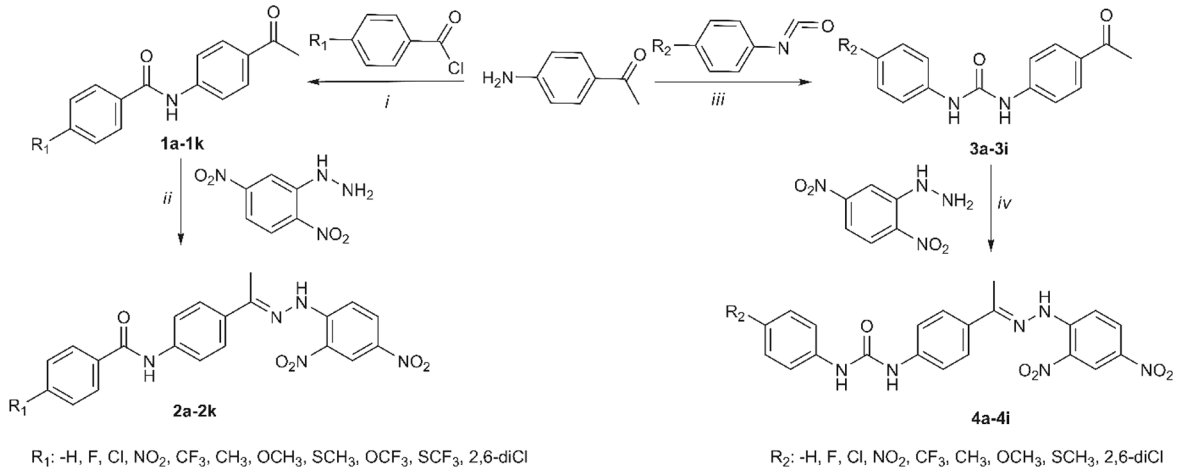

Fig. 1. The synthesis route of all compounds. Reagents: (i) chloroform, reflux; (ii) methanol, reflux; (iii) dichloromethane, 25 °C; (iv) methanol, reflux.

Table 1
% Inhibition of the synthesized compounds and reference agents against MAO-A and MAO-B enzymes at concentrations of 10^{-3} and 10^{-4} M.

Compounds	MAO-A Inhibition %		MAO-A IC_{50} (μM)	MAO-B Inhibition %		MAO-B IC_{50} (μM)	Selectivity	Selectivity index (SI)
	10^{-3} M	10^{-4} M		10^{-3} M	10^{-4} M			
2a	**89.624 ± 1.105**	**84.104 ± 1.248**	0.207 ± 0.010	43.387 ± 0.985	25.314 ± 0.714	>1000	MAO-A	>4830
2b	61.917 ± 0.965	33.880 ± 0.748	>100	36.935 ± 0.801	30.806 ± 0.722	>1000	MAO-A	>10
2c	76.181 ± 0.995	41.969 ± 0.628	>100	43.015 ± 0.628	28.574 ± 0.525	>1000	MAO-A	>10
2d	58.685 ± 0.812	32.606 ± 0.718	>100	56.613 ± 0.611	23.065 ± 0.470	>100	–	–
2e	55.106 ± 0.633	47.165 ± 0.475	>100	26.515 ± 0.529	20.147 ± 0.708	>1000	MAO-A	>10
2f	57.157 ± 1.057	46.566 ± 0.974	>100	47.581 ± 0.997	27.048 ± 0.816	>1000	MAO-A	>10
2g	41.057 ± 0.633	28.273 ± 0.512	>1000	39.516 ± 0.557	23.519 ± 0.629	>1000	–	–
2h	60.834 ± 0.899	42.282 ± 0.716	>100	56.935 ± 0.475	28.288 ± 0.715	>100	–	–
2i	74.498 ± 1.265	46.871 ± 0.945	>100	58.871 ± 1.052	32.250 ± 0.729	>100	–	–
2j	50.753 ± 0.956	37.704 ± 0.882	>100	31.452 ± 0.628	26.388 ± 0.518	>1000	MAO-A	>10
2k	**88.302 ± 1.289**	**80.745 ± 1.475**	0.187 ± 0.008	38.076 ± 0.629	28.537 ± 0.375	>1000	MAO-A	>5347
4a	**93.552 ± 1.240**	**80.106 ± 1.358**	0.138 ± 0.005	56.518 ± 0.978	20.906 ± 0.880	>100	MAO-A	>724
4b	92.562 ± 1.344	41.187 ± 0.891	>100	65.052 ± 1.107	25.358 ± 0.528	>100	–	–
4c	90.823 ± 1.185	47.206 ± 0.852	>100	67.297 ± 0.926	29.547 ± 0.511	>100	–	–
4d	87.541 ± 1.005	45.658 ± 0.962	>100	71.002 ± 1.125	41.256 ± 0.627	>100	–	–
4e	81.627 ± 0.974	46.493 ± 0.965	>100	64.992 ± 0.875	37.297 ± 0.588	>100	–	–
4f	76.715 ± 1.028	40.282 ± 0.887	>100	69.412 ± 1.066	33.625 ± 0.748	>100	–	–
4 g	93.086 ± 1.066	43.771 ± 0.804	>100	77.615 ± 0.997	31.033 ± 0.622	>100	–	–
4 h	75.105 ± 1.108	42.794 ± 0.875	>100	68.744 ± 1.004	36.638 ± 0.729	>100	–	–
4i	**93.581 ± 1.281**	**87.319 ± 1.059**	0.084 ± 0.003	87.361 ± 1.249	42.218 ± 0.748	>100	MAO-A	>1190
Moclobemide	94.121 ± 2.760	82.143 ± 2.691	6.061 ± 0.262	–	–	–	MAO-A	–
Selegiline	–	–	–	98.258 ± 1.052	96.107 ± 1.165	0.037 ± 0.001	MAO-B	–

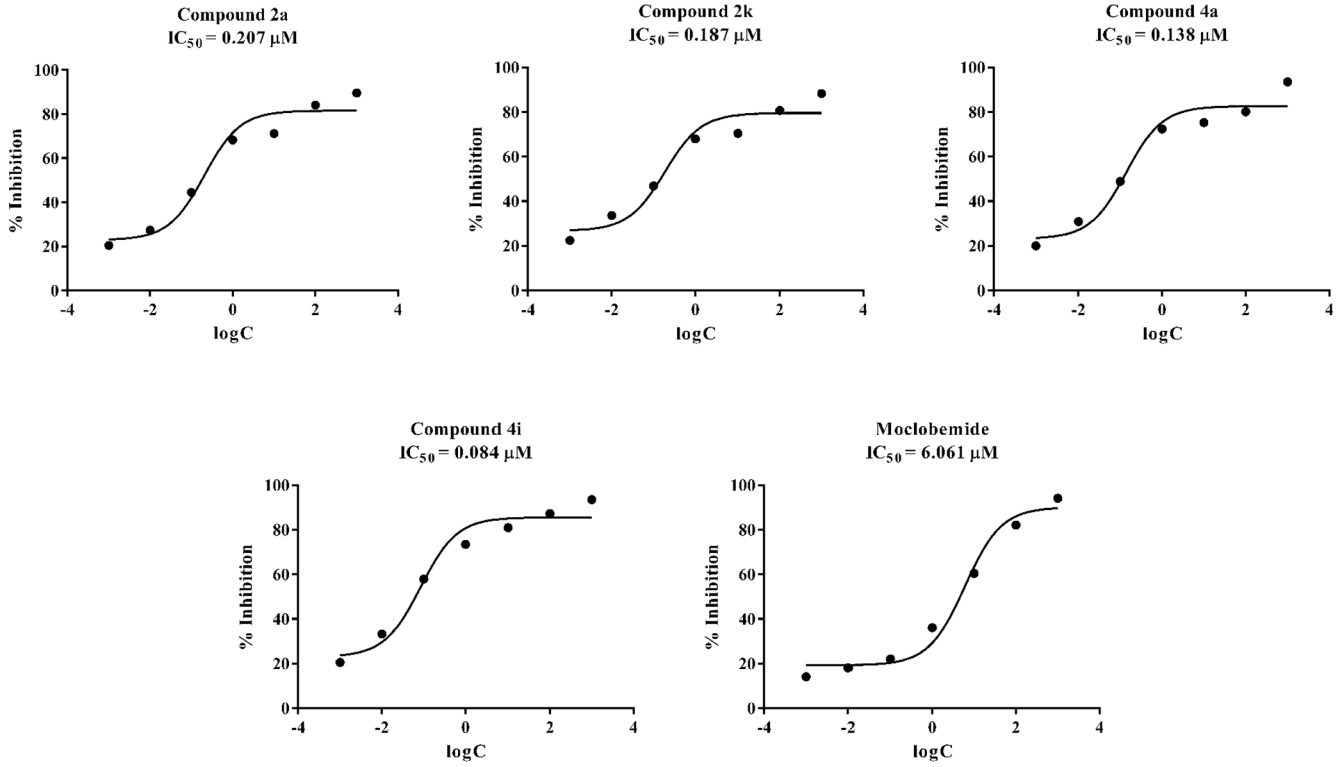

Fig. 2. IC_{50} curves and values of **2a**, **2k**, **4a**, **4i** and moclobemide against MAO-A.

were reported in the absence and presence of compound **4i**. In each case, the initial velocity measurements were collected at various concentrations of substrates (tyramine) varying from 20 μM to 0.625 μM. Thus, linear Lineweaver-Burk graphs could be formed (Fig. 3-**A**). The secondary plot of slope (K_m / V_{max}) versus varying concentrations (0, IC_{50}/2, IC_{50}, and 2(IC_{50})) (Fig. 3-**B**) was formed to measure the K_i value of this compound.

According to Lineweaver-Burk plots, reversible and irreversible inhibition type constitute two general categories. Mixed-type, uncompetitive, competitive, and noncompetitive inhibition types are included in the reversible inhibition [22–26]. As seen in the Lineweaver-Burk plot of compound **4i** (Fig. 3), the lines were intersected on the y-axis, and their slopes and x-intercepts were different. This observation indicated that compound **4i** was a reversible and competitive inhibitor with similar inhibition features as the substrates. The K_i value of compound **4i** was calculated as 0.020 μM with the help of a secondary plot.

2.4. Cytotoxicity test

Compounds **2a**, **2k**, **4a** and **4i** displayed potent MAO-A inhibition

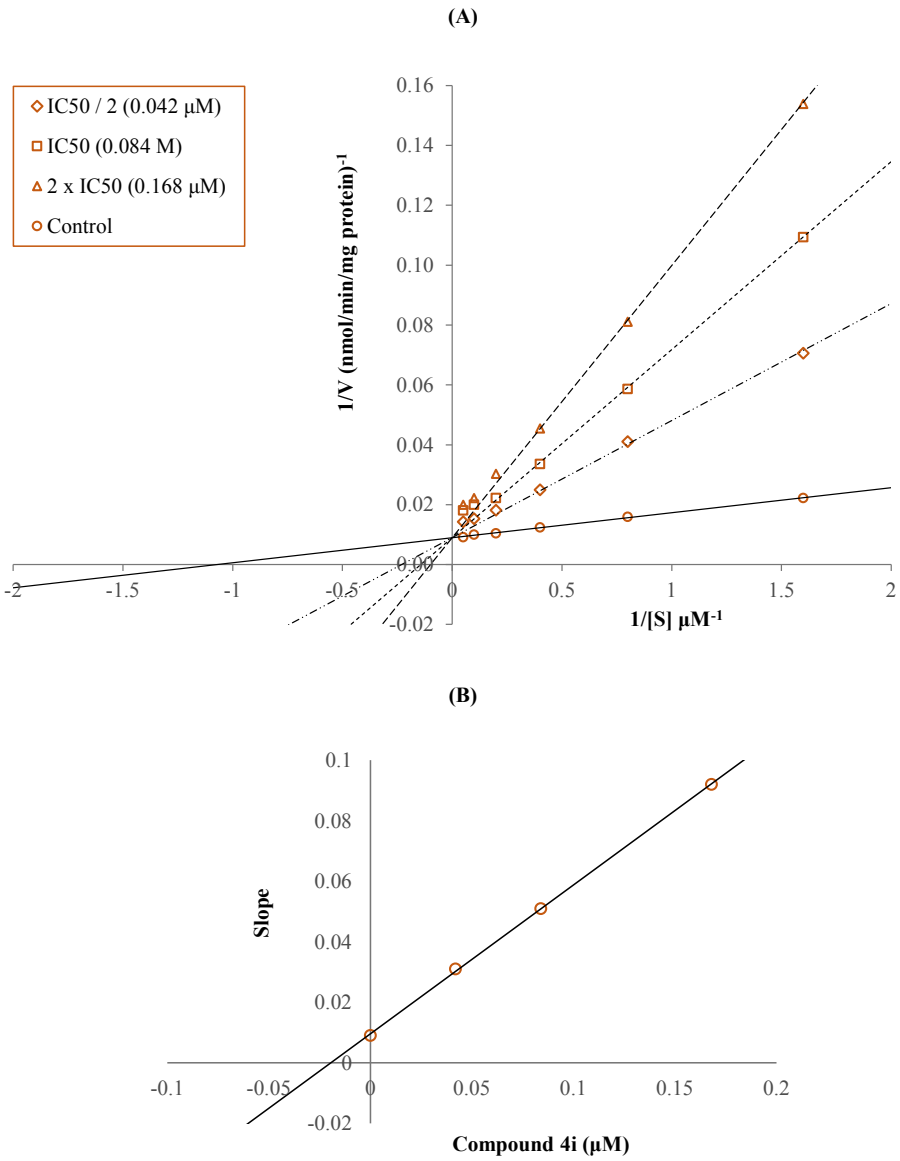

Fig. 3. (A) Lineweaver–Burk plots for the inhibition of *h*MAO A by compound **4i**. [S], substrate concentration (µM); V, reaction velocity (nmol/min/mg protein). Inhibitor concentrations are shown at the left. K_m values from 2 × IC_{50} to control; 10.230, 5.667, 3.417 and 1.015 (µM). V_{max} value of the competitive inhibition; 111.110 ± 2.508 (nmol/min/mg protein). **(B)** Secondary plot for the calculation of the steady-state inhibition constant (K_i) of compound **4i**. K_i was calculated as 0.020 µM.

profile and were further tested for toxicity using the MTT assay in the NIH/3T3 cell line; the IC_{50} values of these compounds are shown in Table 2. Compounds **2a**, **2k**, **4a** and **4i** had the IC_{50} values of 68.208 ± 1.421 µM, 63.960 ± 2.789 µM, 75.225 ± 2.899 µM and 127.660 ± 4.283 µM, respectively, against NIH/3T3 cells. As seen in Table 2, these values were very higher than their IC_{50} values on MAO-A enzyme. Consequently, compounds **2a**, **2k**, **4a** and **4i** were found to be non-cytotoxic at their effective concentrations against MAO-A. This result further increases the importance of the related compounds in terms of medicinal chemistry.

Table 2
The IC_{50} value of the compounds **2a**, **2k**, **4a** and **4i** against NIH/3T3 cell line.

Compounds	IC_{50}(µM) NIH/3T3 cell line	IC_{50}(µM) MAO-A enzyme
2a	68.208 ± 1.421	0.207 ± 0.010
2k	63.960 ± 2.789	0.187 ± 0.008
4a	75.225 ± 2.899	0.138 ± 0.005
4i	127.660 ± 4.283	0.084 ± 0.003

2.5. Prediction of ADME parameters

The absorption, distribution, metabolism and elimination (ADME) properties explain the ability of compounds to reach the target protein and be easily eliminated from the body. The computational approach to drug design greatly helps to reduce the cost and time of subjecting various compounds to molecular analyzes. For this purpose, the Schrödinger *QikProp* [27] program designed by William L. Jorgensen was used to predict physically important identifiers and pharmaceutically relevant properties (ADME) of the synthesized compounds. In addition to predicting molecular properties, this program provides ranges to compare the properties of a particular molecule with the properties of 95% of known drugs [28,29]. The predicted parameters and their recommended values are presented in Table 3.

The "Rule of Five" by Lipinski and the "Rule of Three" by Jorgensen were used to analyze the drug-likeness features of the compounds [30–33]. These rules specify the structural features found in a candidate compound that can be a pharmaceutical product [30–33]. Table 3 showed that all parameters were within the standard ranges and the compounds did not cause more than one violation in terms of "Rule of Five" and "Rule of Three". As a result, based on the findings of the ADME

Table 3
Calculated ADME parameters.

Comp.	MW	RB	DM	MV	DHB	AHB	PSA	logP	logS	PCaco	logBB	PMDCK	PM	CNS	%HOA	VRF	VRT
2a	419.396	8	16.38	1291.918	2	6.5	150.454	3.269	−6.01	40.282	−2.732	15.369	4	−2	74.814	0	1
2b	437.386	8	14.136	1308.03	2	6.5	150.462	3.502	−6.371	40.274	−2.638	27.785	4	−2	76.178	0	1
2c	453.841	8	14.315	1336.036	2	6.5	150.459	3.757	−6.738	40.277	−2.61	37.912	4	−2	77.67	0	1
2d	464.393	9	5.223	1374.318	2	7.5	199.12	2.577	−6.275	4.14	−4.091	1.314	5	−2	40.12	1	2
2e	487.394	8	10.425	1388.746	2	6.5	150.453	4.234	−7.417	40.282	−2.553	67.333	4	−2	80.464	0	1
2f	433.423	8	14.326	1350.856	2	6.5	150.453	3.565	−6.556	40.282	−2.799	15.369	5	−2	76.548	0	1
2g	449.422	9	13.427	1359.698	2	7.25	158.935	3.316	−6.144	40.282	−2.837	15.369	5	−2	62.131	1	1
2h	465.483	9	12.103	1409.287	2	7	150.453	3.886	−6.941	40.282	−2.801	27.557	4	−2	78.426	0	1
2i	503.394	9	11.407	1397.827	2	6.5	158.92	4.294	−7.287	40.282	−2.6	67.78	5	−2	54.898	2	1
2j	519.454	9	10.058	1443.472	2	6.5	150.453	4.703	−7.866	41.415	−2.56	105.335	4	−2	70.468	1	1
2k	488.286	8	17.802	1375.545	2	6.5	147.708	4.239	−7.265	52.377	−2.393	88.193	4	−2	82.534	0	1
4a	434.41	8	16.907	1309.174	3	6	159.752	2.631	−5.911	23.474	−2.949	10.103	5	−2	53.92	1	1
4b	452.401	8	16.972	1325.218	3	6	159.754	2.863	−6.269	23.475	−2.857	18.268	4	−2	55.279	1	1
4c	468.855	8	17.008	1353.246	3	6	159.753	3.116	−6.635	23.475	−2.831	24.925	4	−2	56.765	1	1
4d	479.408	9	11.544	1391.573	3	7	208.418	1.952	−6.207	2.413	−4.323	0.864	5	−2	32.263	1	2
4e	502.409	8	12.666	1406.011	3	6	159.752	3.592	−7.31	23.474	−2.778	44.264	4	−2	46.59	2	1
4f	448.437	8	14.844	1368.111	3	6	159.752	2.924	−6.451	23.474	−3.021	10.103	5	−2	55.64	1	1
4g	464.437	9	13.639	1376.954	3	6.75	168.233	2.688	−6.068	23.474	−3.058	10.103	5	−2	54.256	1	1
4h	480.497	9	12.729	1426.543	3	6.5	159.752	3.251	−6.851	23.474	−3.027	18.115	4	−2	57.554	1	1
4i	503.301	8	18.112	1398.746	3	6	159.644	3.673	−7.035	29.87	−2.564	65.59	5	−2	48.94	2	1

MW: Molecular weight **RB:** Number of rotatable bonds (recommended value: 0–15) **DM:** Computed dipole moment (recommended value: 1–12.5) **MV:** Total solvent-accessible volume (recommended value: 500–2000) **DHB:** Estimated number of hydrogen bond donors (recommended value: 0–6) **AHB:** Estimated number of hydrogen bond acceptors (recommended value: 2–20) **PSA:** Van der Waals surface area of polar nitrogen and oxygen atoms and carbonyl carbon atoms (recommended value: 7–200) **logP:** Predicted octanol/water partition coefficient (recommended value: −2–6.5) **logS:** Predicted aqueous solubility (recommended value: −6.5–0.5) **PCaco:** Predicted apparent Caco-2 cell permeability (recommended value: <25 poor, >500 great) **logBB:** Predicted brain/blood partition coefficient (recommended value: −3–1.2) **PMDCK:** Predicted apparent MDCK cell permeability (recommended value: <25 poor, >500 great) **PM:** Number of likely metabolic reactions (recommended value: 1–8) **CNS:** Predicted central nervous system activity (recommended value: –2 (inactive), +2 (active)) **%HOA:** Predicted human oral absorption percent (recommended value: >80% is high, <25% is poor) **VRF:** Number of violations of Lipinski's rule of five. The rules are: MW < 500, logP < 5, DHB ≤ 5, AHB ≤ 10, Positive PSA value. **VRT:** Number of violations of Jorgensen's rule of three. The three rules are: logS > -5.7, PCaco > 22 nm/s, PM < 7.

parameter trials, the synthesized compounds (**2a**-**4i**) have good and promising pharmacokinetic profiles and could be appropriate for clinical usage.

2.6. Molecular docking studies

As mentioned in MAO inhibition assay, compounds **2a**, **2k**, **4a** and, **4i** were found as the most active derivatives in the series against the *h*MAO-A enzyme. Compound **4i**, with an IC_{50} value of 0.084 ± 0.003 μM, was determined to be the most potent agent among these compounds. Therefore, docking studies were carried out to evaluate its inhibition capability as *in silico*. By using the X-ray crystal structure of *h*MAO-A (PDB ID: 2Z5X) [34] docking studies have been performed and binding modes of compound **4i** were assigned. The docking poses of this compound are presented in Figs. 4–7.

Compound **4i** adequately binds to amino acid residues lining the cavity and is located very near the FAD cofactor. When analyzed docking poses of this compound, it is seen that there are all types of interactions such as π-π, cation-π interactions, the formation of hydrogen bonds. Compound **4i** has nitro groups at the 2nd and 4th positions of the phenyl ring. Among them, the nitrogen atom in the nitro group at the 4th position of phenyl is in interaction with *para*-hydroxyphenyl of Tyr407 by cation- π interaction. Similarly, the phenyl ring located in the middle of the structure forms a π-π interaction with phenyl of Phe208. Also, it is understood from docking poses that the urea group is very essential for polar interactions. As known that the urea group has a carbonyl and two amino moieties. Each of the amino groups creates hydrogen bonds separately with the carbonyl of Gly110. Another hydrogen bond is observed between the carbonyl of the urea group and the amino of Val210. The main structural difference of compound **4i** from other compounds in the series is that it carries chlorine atoms at the 2nd and 6th positions of phenyl ring as well as urea group. It is clearly sighted in Fig. 5 that halogen atom at the 2nd position establishes a halogen bond with a hydrogen of the amino group of Val210. This additional interaction ensures that it binds more strongly to the active site. Furthermore, all these interactions detected explain why compound **4i** exhibits a stronger inhibition profile than other compounds.

In order to analyze the contribution of van der Waals and electrostatic interactions in binding to the enzyme active site, docking studies have been detailed by using *Glide* according to *Per-Residue Interaction panel*. Figs. 6 and 7 present van der Waals and electrostatic interactions of compound **4i**. It is seen that this compound has favorable van der Waals interactions with Tyr69, Leu97, Phe108, Ile180, Ile207, Phe208, Ser209, Val210, Gln315, Ile325, Ile335, Phe352, Tyr407 and Tyr444, displayed with pink and red colors as described in the user guide of *Glide* [35]. Similarly, promising electrostatic contributions of compound **4i** has been determined with Ala111, Asn181, Ile207, Phe208, Ser209, Val210, Gln215, Ile335 and Thr336 amino acids.

3. Conclusions

Medicinal chemists aimed to contribute to the development of new therapeutic agents that have more efficient, selective, less toxicity and side effects at the treatment of neurodegenerative disorders. Therefore

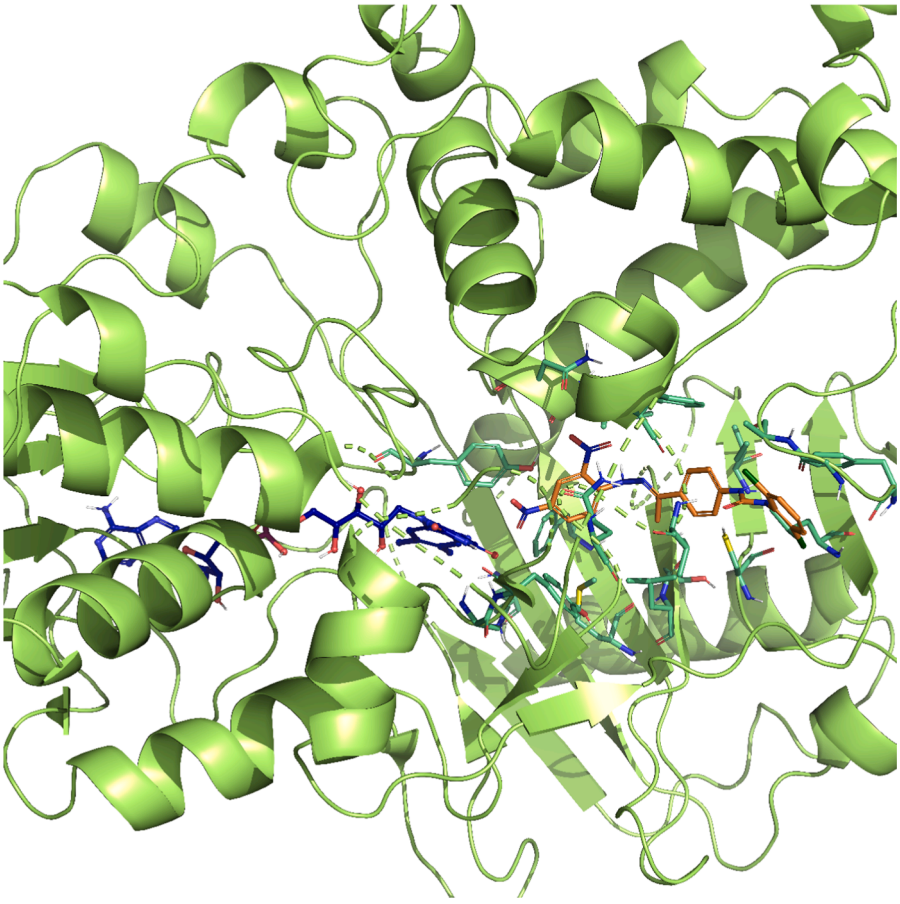

Fig. 4. The three-dimensional pose of compound **4i** in the active region of *h*MAO-A (PDB ID: 2Z5X). The important residues in the active site and this compound are presented by tube model and colored with green and orange, respectively. (For interpretation of the references to colour in this figure legend, the reader is referred to the web version of this article.)

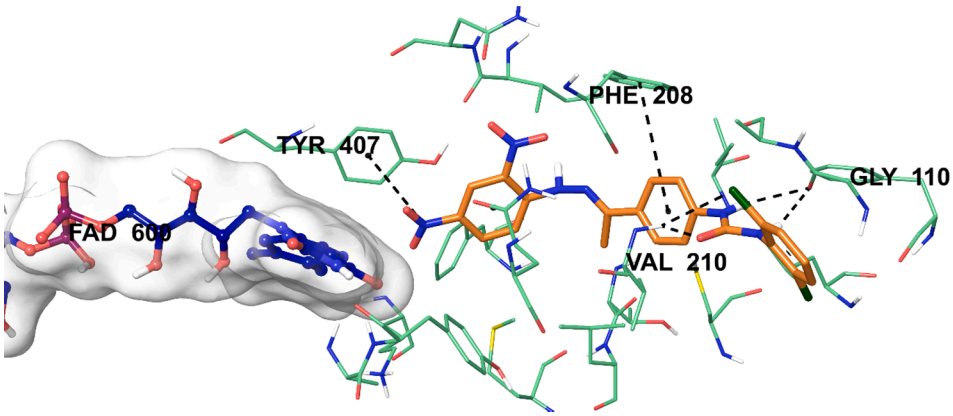

Fig. 5. The three-dimensional interacting mode of compound **4i** in the active region of *h*MAO-A. The inhibitor and the important residues in the active site of the enzyme are presented by tube model. The FAD molecule is colored dark blue with ball and stick model. (For interpretation of the references to colour in this figure legend, the reader is referred to the web version of this article.)

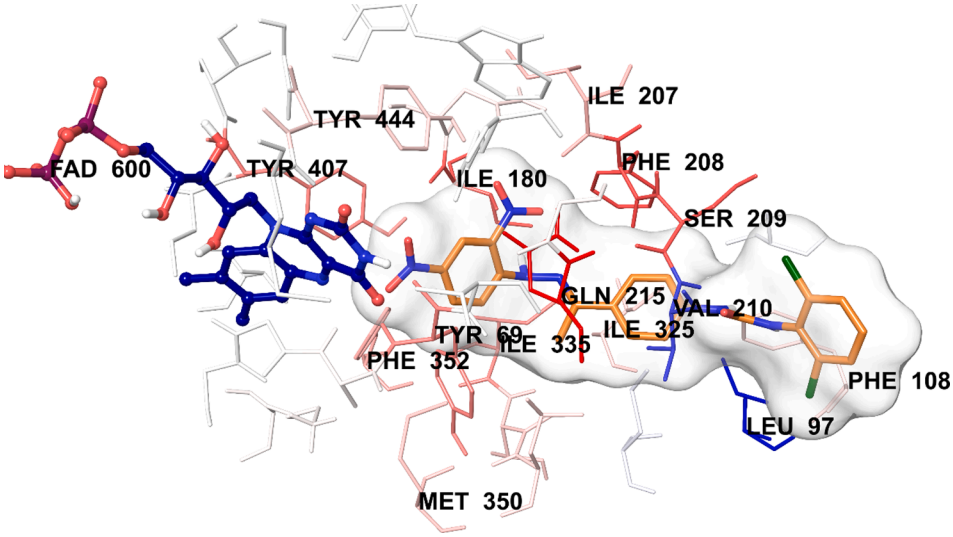

Fig. 6. The van der Waals interaction of compound **4i** with active region of *h*MAO-A. The active ligand has a lot of favourable van der Waals interactions (red and pink). (For interpretation of the references to colour in this figure legend, the reader is referred to the web version of this article.)

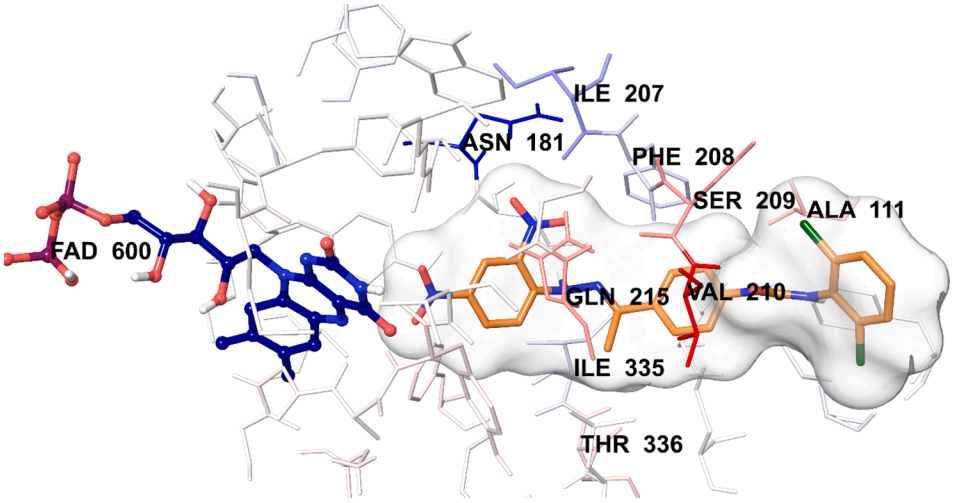

Fig. 7. The electrostatic interaction of compound **4i** with active region of *h*MAO-A. The residues are colored (blue, red, and pink) according to the distance from ligand by Per-Residue Interaction panel. (For interpretation of the references to colour in this figure legend, the reader is referred to the web version of this article.)

we synthesized new hydrazone derivatives bearing urea/amide moieties and evaluated their inhibitory activities on monoamine oxidase enzymes (MAO-A and MAO-B). Compounds **2a** and **4a** including a nonsubstituted phenyl ring and compounds **2k** and **4i** containing 2,6-dichlorophenyl ring exhibited excellent activity against MAO-A. The toxicological and ADME studies ensured the good bioavailability and safety of these compounds. The docking studies represented the binding modes of compounds to enzyme active site. These findings probably will have a good impact on medicinal chemists to synthesize similar compounds in order to discover new agents against depression.

4. Experimental

4.1. General information

Chemicals and solvents used in the study were purchased from Sigma Aldrich (St. Louis, MO, USA) and Merck (Darmstadt, Germany). Thin layer chromatography (TLC) applications performed on silica gel (Kieselgel 60, F254) were used for monitoring reactions and chemical purities of the compounds. Melting points of synthesized compounds were determined by Schmelzpunktbestimmer SMP II and were uncorrected. Infrared spectra were recorded on a Shimadzu FTIR 8400 S Spectrometer. ^{1}H NMR and ^{13}C NMR spectra were recorded in deuterated DMSO using Bruker ACP 200 spectrometer (Bruker Bioscience, Billerica, MA, USA) at 300 MHz and 75 MHz, respectively. It was used tetramethylsilane (TMS) as an internal standard. High-resolution mass spectrometry was carried out on an LCMS-IT-TOF system (Shimadzu).

4.2. Chemistry

4.2.1. The general procedure of amide synthesis

1 mmol *4-aminoacetophenone* was dissolved in 10 mL chloroform and added into the round bottom flask. Then, 1 mmol benzoyl chloride derivatives were added into the flask and the solution was stirred and heated in a water bath for 8–10 h. After completion of the reaction, amide derivatives precipitated and they were filtered and recrystallized from methanol [36].

4.2.2. The general procedure of urea synthesis

1 mmol *4-aminoacetophenone* was dissolved in 10 mL dichloromethane. To a solution of substituted phenyl isocyanate (1 mmol) in CH_2Cl_2 was added to reaction liquid. The mixture was stirred at 25 °C for 8 h. After evaporation of the solvent, the precipitated product was filtered and recrystallized from acetone [37].

4.2.3. The general procedure of hydrazone synthesis

1 mmol *N-(4-acetylphenyl)-4-substitutedbenzamide* was treated with 2 mmol *o,p-dinitrophenyl hydrazine* in 10 mL methanol. The mixture was stirred and heated with dilute sulphuric acid (0.5 mL) under reflux for 10 h. Finally, the reaction was neutralized with water and the precipitated compound was filtered and recrystallized from methanol [38].

4.2.4. N-(4-(1-(2-(2,4-Dinitrophenyl)hydrazono)ethyl)phenyl)benzamide (2a)

Yield: 82%, M.P. = 222–223 °C, FTIR (ATR, cm^{-1}): 3308 (N—H), 3095 (=C—H), 2989 (C—H), 1653 (C=O), 1620 (C=N), 1597, 1573 (C=C), 1506 (NO_2 *asym*), 1300 (NO_2 *sym*), 825 (=C—H). ^{1}H NMR (300 MHz, DMSO-d_6): δ 2.43 (s, 3H, CH_3), 7.54–8.87 (m, 12H, Ar—H), 10.44 (s, 1H, CO=NH), 11.10 (s, 1H, hydrazone NH). ^{13}C NMR (75 MHz, DMSO-d_6): δ 13.58, 117.03, 120.25, 123.50, 127.56, 128.19, 128.89, 130.02, 130.57, 132.22, 132.37, 135.18, 137.60, 141.38, 144.86, 153.29, 166.17. HRMS (*m/z*): $[M + H]^+$ calcd for $C_{21}H_{17}N_5O_5$: 420.1302; found: 420.1303.

4.2.5. N-(4-(1-(2-(2,4-Dinitrophenyl)hydrazono)ethyl)phenyl)-4-fluorobenzamide (2b)

Yield: 77%, M.P. = 252–253 °C, FTIR (ATR, cm^{-1}): 3394, 3308 (N—H), 3091 (=C—H), 2931 (C—H), 1670 (C=O), 1649 (C=N), 1599, 1585 (C=C), 1500 (NO_2 *asym*), 1327 (NO_2 *sym*), 831 (=C—H). ^{1}H NMR (300 MHz, DMSO-d_6): δ 2.45 (s, 3H, CH_3), 7.36–8.90 (m, 11*H*, Ar—H), 10.47 (s, 1H, CO=NH), 11.12 (s, 1H, hydrazone NH). ^{13}C NMR (75 MHz, DMSO-d_6): δ 13.66, 115.72, 116.01, 117.05, 120.34, 123.53, 127.60, 130.09, 130.59, 130.91, 131.04, 131.59, 132.50, 137.63, 141.27, 144.89, 153.36, 162.99, 166.28. HRMS (*m/z*): $[M-H]^-$ calcd for $C_{21}H_{16}N_5O_5F$: 436.1063; found: 436.1052.

4.2.6. N-(4-(1-(2-(2,4-Dinitrophenyl)hydrazono)ethyl)phenyl)-4-chlorobenzamide (2c)

Yield: 85%, M.P. = 264–265 °C, FTIR (ATR, cm^{-1}): 3315 (N—H), 3101 (=C—H), 2974 (C—H), 1656 (C=O), 1618 (C=N), 1591, 1533 (C=C), 1516 (NO_2 *asym*), 1301 (NO_2 *sym*), 825 (=C—H). ^{1}H NMR (300 MHz, DMSO-d_6): δ 2.45 (s, 3H, CH_3), 7.61–8.89 (m, 11*H*, Ar—H), 10.51 (s, 1H, CO=NH), 11.12 (s, 1H, hydrazone NH). ^{13}C NMR (75 MHz, DMSO-d_6): δ 13.65, 117.05, 120.37, 123.53, 127.61, 128.98, 130.18, 130.60, 132.59, 133.59, 133.85, 137.07, 137.64, 141.16, 144.88, 153.33, 165.05. HRMS (*m/z*): $[M-H]^-$ calcd for $C_{21}H_{16}N_5O_5Cl$: 452.0767; found: 452.0745.

4.2.7. N-(4-(1-(2-(2,4-Dinitrophenyl)hydrazono)ethyl)phenyl)-4-nitrobenzamide (2d)

Yield: 76%, M.P. = 213–214 °C, FTIR (ATR, cm^{-1}): 3404, 3296 (N—H), 3088 (=C—H), 2985 (C—H), 1680 (C=O), 1602 (C=N), 1585, 1573 (C=C), 1516 (NO_2 *asym*), 1300 (NO_2 *sym*), 829 (=C—H). ^{1}H NMR (300 MHz, DMSO-d_6): δ 2.41 (s, 3H, CH_3), 7.63–8.85 (m, 11*H*, Ar—H), 10.72 (s, 1H, CO=NH), 11.08 (s, 1H, hydrazone NH). ^{13}C NMR (75 MHz, DMSO-d_6): δ 13.32, 113.72, 116.82, 120.37, 123.46, 124.03, 127.59, 129.34, 130.46, 132.82, 136.92, 137.62, 140.83, 144.81, 149.66, 151.53, 153.08, 154.61, 164.45. HRMS (*m/z*): $[M + H]^+$ calcd for $C_{21}H_{16}N_6O_7$: 465.1153; found: 465.1154.

4.2.8. N-(4-(1-(2-(2,4-Dinitrophenyl)hydrazono)ethyl)phenyl)-4-(trifluoromethyl)benzamide (2e)

Yield: 79%, M.P. = 204–205 °C, FTIR (ATR, cm^{-1}): 3317 (N—H), 3057 (=C—H), 2980 (C—H), 1656 (C=O), 1616 (C=N), 1599 (C=C), 1519 (NO_2 *asym*), 1301 (NO_2 *sym*), 825 (=C—H). ^{1}H NMR (300 MHz, DMSO-d_6): δ 2.44 (s, 3H, CH_3), 7.88–8.88 (m, 11*H*, Ar—H), 10.65 (s, 1H, CO=NH), 11.10 (s, 1H, hydrazone NH). ^{13}C NMR (75 MHz, DMSO-d_6): δ 13.59, 117.03, 120.39, 122.57, 123.49, 125.87, 125.92, 127.61, 129.14, 130.06, 130.58, 131.7, 132.15, 132.75, 137.64, 138.96, 140.98, 144.86, 153.21, 164.99. HRMS (*m/z*): $[M + H]^+$ calcd for $C_{22}H_{16}N_5O_5F_3$: 488.1176; found: 488.1154.

4.2.9. N-(4-(1-(2-(2,4-Dinitrophenyl)hydrazono)ethyl)phenyl)-4-methylbenzamide (2f)

Yield: 88%, M.P. = 183–184 °C, FTIR (ATR, cm^{-1}): 3363, 3311 (N—H), 3064 (=C—H), 2928 (C—H), 1645 (C=O), 1614 (C=N), 1593, 1573 (C=C), 1516 (NO_2 *asym*), 1301 (NO_2 *sym*), 825 (=C—H). ^{1}H NMR (300 MHz, DMSO-d_6): δ 2.39 (s, 3H, CH_3), 2.42 (s, 3H, CH_3), 7.32–8.85 (m, 11*H*, Ar—H), 10.34 (s, 1H, CO=NH), 11.09 (s, 1H, hydrazone NH). ^{13}C NMR (75 MHz, DMSO-d_6): δ 13.65, 21.51, 117.04, 120.28, 123.56, 127.58, 128.24, 129.42, 130.05, 130.60, 131.13, 132.26, 137.61, 141.47, 142.30, 144.88, 153.47, 165.96. HRMS (*m/z*): $[M-H]^-$ calcd for $C_{22}H_{19}N_5O_5$: 432.1313; found: 432.1293.

4.2.10. N-(4-(1-(2-(2,4-Dinitrophenyl)hydrazono)ethyl)phenyl)-4-methoxybenzamide (2g)

Yield: 79%, M.P. = 146–147 °C, FTIR (ATR, cm^{-1}): 3365, 3311 (N—H), 3099 (=C—H), 2933 (C—H), 1645 (C=O), 1616 (C=N), 1593, 1556 (C=C), 1516 (NO_2 *asym*), 1303 (NO_2 *sym*), 831 (=C—H). ^{1}H NMR (300 MHz, DMSO-d_6): δ 2.44 (s, 3H, CH_3), 3.84 (s, 3H, OCH_3), 7.06–8.89

(m, 11*H*, Ar—H), 10.28 (s, 1H, CO═NH), 11.12 (s, 1H, hydrazone NH). ^{13}C NMR (75 MHz, DMSO-d_6): δ 13.61, 55.94, 114.10, 117.04, 120.53, 127.14, 127.55, 130.04, 130.17, 130.58, 132.15, 137.59, 141.60, 144.88, 153.42, 162.50, 165.49. HRMS (*m/z*): $[M-H]^-$ calcd for $C_{22}H_{19}N_5O_6$: 448.1263; found: 448.1245.

4.2.11. N-(4-(1-(2-(2,4-Dinitrophenyl)hydrazono)ethyl)phenyl)-4-(methylthio)benzamide (**2h**)

Yield: 68%, M.P. = 166–167 °C, FTIR (ATR, cm^{-1}): 3309 (N—H), 3095 (═C—H), 2922 (C—H), 1645 (C═O), 1616 (C═N), 1591, 1573 (C═C), 1512 (NO_2 *asym*), 1301 (NO_2 *sym*), 825 (═C—H). ^{1}H NMR (300 MHz, DMSO-d_6): δ 2.45 (s, 3H, CH_3), 2.54 (s, 3H, SCH_3), 7.38–8.89 (m, 11*H*, Ar—H), 10.39 (s, 1H, CO═NH), 11.12 (s, 1H, hydrazone NH). ^{13}C NMR (75 MHz, DMSO-d_6): δ 13.63, 14.52, 117.05, 120.31, 123.54, 125.29, 127.59, 130.07, 130.60, 130.93, 132.33, 137.61, 141.42, 143.89, 144.88, 153.40, 165.51. HRMS (*m/z*): $[M-H]^-$ calcd for $C_{22}H_{19}N_5O_5S$: 464.1034; found: 464.1046.

4.2.12. N-(4-(1-(2-(2,4-Dinitrophenyl)hydrazono)ethyl)phenyl)-4-(trifluoromethoxy)benzamide (**2i**)

Yield: 75%, M.P. = 197–198 °C, FTIR (ATR, cm^{-1}): 3309 (N—H), 3095 (═C—H), 2920 (C—H), 1651 (C═O), 1616 (C═N), 1593, 1575 (C═C), 1516 (NO_2 *asym*), 1303 (NO_2 *sym*), 823 (═C—H). ^{1}H NMR (300 MHz, DMSO-d_6): δ 2.44 (s, 3H, CH_3), 7.53–8.88 (m, 11*H*, Ar—H), 10.54 (s, 1H, CO═NH), 11.11 (s, 1H, hydrazone NH). ^{13}C NMR (75 MHz, DMSO-d_6): δ 13.60, 117.03, 120.30, 121.19, 122.15, 123.50, 127.60, 130.06, 130.62, 132.59, 134.30, 137.63, 141.14, 144.86, 151.01, 153.26, 164.95. HRMS (*m/z*): $[M+H]^+$ calcd for $C_{22}H_{16}N_5O_6F_3$: 504.1125; found: 504.1123.

4.2.13. N-(4-(1-(2-(2,4-Dinitrophenyl)hydrazono)ethyl)phenyl)-4-(trifluoromethylthio)benzamide (**2j**)

Yield: 74%, M.P. = 208–209 °C, FTIR (ATR, cm^{-1}): 3317 (N—H), 3102 (═C—H), 2968 (C—H), 1645 (C═O), 1616 (C═N), 1595, 1579 (C═C), 1512 (NO_2 *asym*), 1301 (NO_2 *sym*), 831 (═C—H). ^{1}H NMR (300 MHz, DMSO-d_6): δ 2.45 (s, 3H, CH_3), 7.88–8.90 (m, 11*H*, Ar—H), 10.64 (s, 1H, CO═NH), 11.12 (s, 1H, hydrazone NH). ^{13}C NMR (75 MHz, DMSO-d_6): δ 13.63, 117.04, 120.35, 123.52, 127.18, 127.64, 130.12, 130.59, 132.74, 136.37, 137.66, 137.88, 141.05, 144.88, 153.28, 165.24. HRMS (*m/z*): $[M+H]^+$ calcd for $C_{22}H_{16}N_5O_5F_3S$: 520.0897; found: 520.0907.

4.2.14. 2,6-Dichloro-N-(4-(1-(2-(2,4-dinitrophenyl)hydrazono)ethyl)phenyl)benzamide (**2k**)

Yield: 78%, M.P. = 273–274 °C, FTIR (ATR, cm^{-1}): 3309 (N—H), 3090 (═C—H), 2918 (C—H), 1645 (C═O), 1608 (C═N), 1587, 1573 (C═C), 1504 (NO_2 *asym*), 1301 (NO_2 *sym*), 831 (═C—H). ^{1}H NMR (300 MHz, DMSO-d_6): δ 2.42 (s, 3H, CH_3), 7.49–8.85 (m, 10*H*, Ar—H), 10.98 (s, 1H, CO═NH), 11.08 (s, 1H, hydrazone NH). ^{13}C NMR (75 MHz, DMSO-d_6): δ 13.57, 116.97, 117.05, 119.62, 123.42, 127.82, 128.75, 130.00, 130.53, 131.65, 132.00, 132.94, 136.63, 137.63, 140.59, 144.80, 153.08, 162.68. HRMS (*m/z*): $[M+H]^+$ calcd for $C_{21}H_{15}N_5O_5Cl_2$: 488.0523; found: 488.0501.

4.2.15. 1-(4-(1-(2-(2,4-Dinitrophenyl)hydrazono)ethyl)phenyl)-3-phenylurea (4a)

Yield: 86%, M.P. = 235–236 °C, FTIR (ATR, cm^{-1}): 3311 (N—H), 3097 (═C—H), 2922 (C—H), 1651 (C═O), 1614 (C═N), 1593, 1573 (C═C), 1514 (NO_2 *asym*), 1300 (NO_2 *sym*), 831 (═C—H). ^{1}H NMR (300 MHz, DMSO-d_6): δ 2.44 (s, 3H, CH_3), 6.96–8.91 (m, 14H, Ar—H and urea NH), 11.13 (s, 1H, hydrazone NH). ^{13}C NMR (75 MHz, DMSO-d_6): δ 13.64, 117.03, 118.37, 119.05, 122.57, 123.42, 127.84, 129.19, 130.05, 130.45, 130.98, 137.85, 139.97, 142.10, 145.04, 152.83, 153.82. HRMS (*m/z*): $[M-H]^-$ calcd for $C_{21}H_{18}N_6O_5$: 433.1266; found: 433.1249.

4.2.16. 1-(4-(1-(2-(2,4-Dinitrophenyl)hydrazono)ethyl)phenyl)-3-(4-fluorophenyl)urea (**4b**)

Yield: 78%, M.P. = 255–256 °C, FTIR (ATR, cm^{-1}): 3309 (N—H), 3078 (═C—H), 2954 (C—H), 1645 (C═O), 1614 (C═N), 1593, 1573 (C═C), 1506 (NO_2 *asym*), 1303 (NO_2 *sym*), 831 (═C—H). ^{1}H NMR (300 MHz, DMSO-d_6): δ 2.43 (s, 3H, CH_3), 7.10–8.96 (m, 13H, Ar—H and urea NH), 11.12 (s, 1H, hydrazone NH). ^{13}C NMR (75 MHz, DMSO-d_6): δ 13.67, 115.52, 115.81, 117.02, 118.40, 120.80, 120.90, 123.41, 127.81, 130.22, 130.43, 131.00, 136.27, 137.77, 142.06, 145.04, 152.92, 153.78, 159.70, 162.47. HRMS (*m/z*): $[M-H]^-$ calcd for $C_{21}H_{17}N_6O_5F$: 451.1172; found: 451.1150.

4.2.17. 1-(4-(1-(2-(2,4-Dinitrophenyl)hydrazono)ethyl)phenyl)-3-(4-chlorophenyl)urea (**4c**)

Yield: 75%, M.P. = 275–276 °C, FTIR (ATR, cm^{-1}): 3311 (N—H), 3090 (═C—H), 2976 (C—H), 1645 (C═O), 1616 (C═N), 1591, 1575 (C═C), 1506 (NO_2 *asym*), 1301 (NO_2 *sym*), 829 (═C—H). ^{1}H NMR (300 MHz, DMSO-d_6): δ 2.43 (s, 3H, CH_3), 7.32–8.99 (m, 13H, Ar—H and urea NH), 11.11 (s, 1H, hydrazone NH). ^{13}C NMR (75 MHz, DMSO-d_6): δ 13.61, 116.95, 118.23, 120.30, 123.56, 126.02, 127.89, 129.12, 129.99, 130.59, 130.80, 137.52, 138.95, 141.87, 144.88, 152.65, 153.59. HRMS (*m/z*): $[M+H]^+$ calcd for $C_{21}H_{17}N_6O_5Cl$: 469.1022; found: 469.0993.

4.2.18. 1-(4-(1-(2-(2,4-Dinitrophenyl)hydrazono)ethyl)phenyl)-3-(4-nitrophenyl)urea (**4d**)

Yield: 80%, M.P. = 215–216 °C, FTIR (ATR, cm^{-1}): 3394, 3308 (N—H), 3091 (═C—H), 2989 (C—H), 1670 (C═O), 1619 (C═N), 1599, 1585 (C═C), 1500 (NO_2 *asym*), 1327 (NO_2 *sym*), 831 (═C—H). ^{1}H NMR (300 MHz, DMSO-d_6): δ 2.45 (s, 3H, CH_3), 7.58–9.33 (m, 13H, Ar—H and urea NH), 11.07 (s, 1H, hydrazone NH). HRMS (*m/z*): $[M-H]^-$ calcd for $C_{21}H_{17}N_7O_7$: 478.1117; found: 478.1098.

4.2.19. 1-(4-(1-(2-(2,4-Dinitrophenyl)hydrazono)ethyl)phenyl)-3-(4-(trifluoromethyl)phenyl)urea (**4e**)

Yield: 75%, M.P. = 238–239 °C, FTIR (ATR, cm^{-1}): 3360, 3306 (N—H), 3101 (═C—H), 2926 (C—H), 1674 (C═O), 1614 (C═N), 1587, 1575 (C═C), 1504 (NO_2 *asym*), 1301 (NO_2 *sym*), 829 (═C—H). ^{1}H NMR (300 MHz, DMSO-d_6): δ 2.35 (s, 3H, CH_3), 7.54–8.99 (m, 13H, Ar—H and urea NH), 11.05 (s, 1H, hydrazone NH). ^{13}C NMR (75 MHz, DMSO-d_6): δ 13.36, 113.96, 117.00, 118.61, 123.37, 123.49, 124.69, 126.46, 127.81, 128.43, 130.19, 130.41, 131.35, 137.80, 141.61, 143.72, 145.00, 152.56, 153.63. HRMS (*m/z*): $[M-H]^-$ calcd for $C_{22}H_{17}N_6O_5F_3$: 501.1140; found: 501.1125.

4.2.20. 1-(4-(1-(2-(2,4-Dinitrophenyl)hydrazono)ethyl)phenyl)-3-(4-methylphenyl)urea (**4f**)

Yield: 78%, M.P. = 201–202 °C, FTIR (ATR, cm^{-1}): 3311, 3308 (N—H), 3095 (═C—H), 2933 (C—H), 1651 (C═O), 1620 (C═N), 1589, 1573 (C═C), 1504 (NO_2 *asym*), 1300 (NO_2 *sym*), 827 (═C—H). ^{1}H NMR (300 MHz, DMSO-d_6): δ 2.24 (s, 3H, CH_3), 2.43 (s, 3H, CH_3), 7.08–8.91 (m, 13H, Ar—H and urea NH), 11.12 (s, 1H, hydrazone NH). ^{13}C NMR (75 MHz, DMSO-d_6): δ 13.61, 20.84, 116.96, 118.07, 118.87, 123.59, 127.90, 129.68, 130.54, 130.61, 131.37, 136.49, 137.33, 137.50, 142.17, 144.90, 152.78, 153.69. HRMS (*m/z*): $[M-H]^-$ calcd for $C_{22}H_{20}N_6O_5$: 447.1422; found: 447.1405.

4.2.21. 1-(4-(1-(2-(2,4-Dinitrophenyl)hydrazono)ethyl)phenyl)-3-(4-methoxyphenyl)urea (**4g**)

Yield: 81%, M.P. = 192–193 °C, FTIR (ATR, cm^{-1}): 3358, 3298 (N—H), 3051 (═C—H), 2916 (C—H), 1674 (C═O), 1614 (C═N), 1589, 1531 (C═C), 1504 (NO_2 *asym*), 1317 (NO_2 *sym*), 823 (═C—H). ^{1}H NMR (300 MHz, DMSO-d_6): δ 2.42 (s, 3H, CH_3), 3.72 (s, 3H, OCH_3), 6.86–8.89 (m, 13H, Ar—H and urea NH), 11.11 (s, 1H, hydrazone NH). ^{13}C NMR (75 MHz, DMSO-d_6): δ 13.59, 55.62, 114.46, 116.94, 118.00, 120.63, 123.57, 127.87, 129.95, 130.42, 130.59, 132.89, 137.48, 142.28, 144.88, 152.92, 153.67, 155.07. HRMS (*m/z*): $[M-H]^-$ calcd for

$C_{22}H_{20}N_6O_6$: 463.1372; found: 463.1378.

4.2.22. 1-(4-(1-(2-(2,4-Dinitrophenyl)hydrazono)ethyl)phenyl)-3-(4-(methylthio)phenyl)urea (**4h**)

Yield: 72%, M.P. = 211–212 °C, FTIR (ATR, cm^{-1}): 3352, 3296 (N—H), 3103 (=C—H), 2989 (C—H), 1674 (C=O), 1614 (C=N), 1583, 1543 (C=C), 1514 (NO_2 *asym*), 1317 (NO_2 *sym*), 844 (=C—H). ^{1}H NMR (300 MHz, DMSO-d_6): δ 2.43 (s, 3H, SCH_3), 2.44 (s, 3H, CH_3), 7.21–8.94 (m, 13H, Ar—H and urea NH), 11.12 (s, 1H, hydrazone NH). ^{13}C NMR (75 MHz, DMSO-d_6): δ 13.61, 16.38, 112.61, 116.95, 118.13, 119.55, 123.57, 127.88, 128.13, 129.97, 130.59, 130.70, 137.50, 137.60, 142.02, 144.88, 152.69, 153.63. HRMS (*m/z*): $[M-H]^-$ calcd for $C_{22}H_{20}N_6O_5S$: 479.1143; found: 479.1123.

4.2.23. 1-(2,6-Dichlorophenyl)-3-(4-(1-(2-(2,4-dinitrophenyl)hydrazono)ethyl)phenyl)urea (**4i**)

Yield: 77%, M.P. = 244–245 °C, FTIR (ATR, cm^{-1}): 3356, 3311 (N—H), 3102 (=C—H), 2901 (C—H), 1674 (C=O), 1614 (C=N), 1585, 1573 (C=C), 1514 (NO_2 *asym*), 1300 (NO_2 *sym*), 831 (=C—H). ^{1}H NMR (300 MHz, DMSO-d_6): 2.43 (s, 3H, CH_3), 7.31–9.27 (m, 12H, Ar—H and urea NH), 11.12 (s, 1H, hydrazone NH). ^{13}C NMR (75 MHz, DMSO-d_6): δ 13.64, 116.99, 118.12, 123.58, 127.88, 128.96, 129.08, 130.01, 130.61, 130.73, 133.57, 134.48, 137.52, 142.11, 144.90, 152.62, 153.64. HRMS (*m/z*): $[M-H]^-$ calcd for $C_{21}H_{16}N_6O_5Cl_2$: 501.0486; found: 501.0465.

4.3. MAO inhibition assay

The *in vitro* MAO inhibition assay was performed using the current fluorometric method and the percentages and IC_{50} values of test compounds were calculated as in previously declared by our research group [22–26].

4.4. MAO enzyme kinetics studies

The same materials used in the MAO inhibition assay were used in this experiment. In accordance with the test given in our previous studies, compound **4i**, which was identified as the most active compound as a result of the MAO inhibition assay, was experienced at three independent concentrations of $IC_{50}/2$, IC_{50} and $2(IC_{50})$ [22–26]. All processes were evaluated in quadruplicate. The results were analyzed with Microsoft Office Excel 2013 using Lineweaver-Burk diagrams. The Vmax values of the Lineweaver-Burk plots were replotted versus the inhibitor concentration, and the K_i values were determined from the x-axis intercept as $-K_i$.

4.5. Cytotoxicity test

The NIH/3T3 mouse embryonic fibroblast cell line (ATCC® CRL-1658 ™, London, UK) was used for cytotoxicity assays. The incubation period of NIH/3T3 cells was based on the supplier's recommendation. NIH/3T3 cells were seeded at $1x10^4$ cells into each well of 96-well plates. MTT assay was carried out in accordance with the standards previously described manner [39,40]. The most effective compounds **2a**, **2k**, **4a** and **4i** were tested between 1 mM and 0.000316 mM concentrations. Inhibition % for each concentration was calculated according to the following formula and IC_{50} values were reported by plotting the % inhibition dose response curve against the compound concentrations tested [39–41].

$$\%\ \text{inhibition} = 100 - (\text{mean sample} \times 100/\text{mean solvent})$$

4.6. Prediction of ADME parameters

In order to estimate the pharmacokinetic profiles of synthesized compounds (**2a**-**4i**) *QikProp 4.8* software [27] was used and their physicochemical parameters were calculated by the *in silico* method.

4.7. Molecular docking

A structure based *in silico* procedure was applied to discover the binding modes of compound **4i** to *h*MAO-A enzyme active site. The crystal structures of *h*MAO-A (PDB ID: 2Z5X) [34], which was crystallized with harmine, were retrieved from the Protein Data Bank server (www.pdb.org). The docking procedure was conducted according to the published papers priorly by our research community [22–26].

Declaration of Competing Interest

The authors declare that they have no known competing financial interests or personal relationships that could have appeared to influence the work reported in this paper.

Appendix A. Supplementary material

The FTIR, ^{1}H-NMR, ^{13}C-NMR, and HR-MS spectrums of compounds **2a**–**2k** and **4a**-**4i** are available online.

Supplementary data to this article can be found online at https://doi.org/10.1016/j.bioorg.2021.105038.

References

[1] A.C. Tripathi, S. Upadhyay, S. Paliwal, S.K. Saraf, Privileged scaffolds as MAO inhibitors: Retrospect and prospects, Eur. J. Med. Chem. 145 (2018) 445–497, https://doi.org/10.1016/j.ejmech.2018.01.003.

[2] A. Samadi, C. Ríos, I. Bolea, M. Chioua, I. Iriepa, I. Moraleda, M. Bartolini, V. Andrisano, E. Gálvez, C. Valderas, M. Unzeta, J. Marco-Contelles, Multipotent MAO and cholinesterase inhibitors for the treatment of Alzheimer's disease: Synthesis, pharmacological analysis and molecular modeling of heterocyclic substituted alkyl and cycloalkyl propargyl amine, Eur. J. Med. Chem. 52 (2012) 251–262, https://doi.org/10.1016/j.ejmech.2012.03.022.

[3] M. D'Ascenzio, P. Chimenti, M.C. Gidaro, C. De Monte, D. De Vita, A. Granese, L. Scipione, R. Di Santo, G. Costa, S. Alcaro, M. Yáñez, S. Carradori, (Thiazol-2-yl) hydrazone derivatives from acetylpyridines as dual inhibitors of MAO and AChE: Synthesis, biological evaluation and molecular modeling studies, J. Enzyme Inhib. Med. Chem. 30 (2015) 908–919, https://doi.org/10.3109/14756366.2014.987138.

[4] M. Garcia-Miralles, J. Ooi, C.F. Bardile, L.J. Tan, M. George, C.L. Drum, R.Y. Lin, M.R. Hayden, M.A. Pouladi, Treatment with the MAO-A inhibitor clorgyline elevates monoamine neurotransmitter levels and improves affective phenotypes in a mouse model of Huntington disease, Exp. Neurol. 278 (2016) 4–10, https://doi.org/10.1016/j.expneurol.2016.01.019.

[5] A. Shetnev, R. Shlenev, J. Efimova, S. Ivanovskii, A. Tarasov, A. Petzer, J.P. Petzer, 1,3,4-Oxadiazol-2-ylbenzenesulfonamides as privileged structures for the inhibition of monoamine oxidase B, Bioorganic Med. Chem. Lett. 29 (2019), 126677, https://doi.org/10.1016/j.bmcl.2019.126677.

[6] R.K.P. Tripathi, S.R. Ayyannan, Design, synthesis, and evaluation of 2-amino-6-nitrobenzothiazole-derived hydrazones as MAO Inhibitors: Role of the methylene spacer group, Chem. Med. Chem. 11 (14) (2016) 1551–1567, https://doi.org/10.1002/cmdc.201600202.

[7] J. Hagenow, S. Hagenow, K. Grau, M. Khanfar, L. Hefke, E. Proschak, H. Stark, Reversible small molecule inhibitors of MAO-A and MAO-B with anilide motifs, Drug Des. Devel. Ther. 14 (2020) 371–393, https://doi.org/10.2147/DDDT.S236586.

[8] B. Vishnu Nayak, S. Ciftci-Yabanoglu, S.S. Jadav, M. Jagrat, B.N. Sinha, G. Ucar, V. Jayaprakash, Monoamine oxidase inhibitory activity of 3,5-biaryl-4,5-dihydro-1H- pyrazole-1-carboxylate derivatives, Eur. J. Med. Chem. 69 (2013) 762–767, https://doi.org/10.1016/j.ejmech.2013.09.010.

[9] M. Bortolato, K. Chen, J.C. Shih, Monoamine oxidase inactivation: from pathophysiology to therapeutics, 60 (2008) 1527–1533. doi: 10.1016/j.addr.2008.06.002.

[10] F. Tok, B. Koçyiğit-Kaymakçıoğlu, B.N. Sağlık, S. Levent, Y. Özkay, Z. A. Kaplancıklı, Synthesis and biological evaluation of new pyrazolone schiff bases as monoamine oxidase and cholinesterase inhibitors, Bioorg. Chem. 84 (2019) 41–50, https://doi.org/10.1016/j.bioorg.2018.11.016.

[11] Ö. Atlı, Y. Özkay, Synthesis and MAO inhibitory activity of novel thiazole-hydrazones, Turk. J. Chem. 41 (2017) 685–699, https://doi.org/10.3906/kim-1612-78.

[12] S.C. Moldoveanu, Pyrolysis of other nitrogen-containing compounds, 2 (2019) 349-390. doi:10.1016/B978-0-444-64000-0.00009-3.

[13] B. Kocyigit-Kaymakcioglu, S.S. Yazıcı, F. Tok, M. Dikmen, S. Engür, E.E. Oruç-Emre, A. İyidoğan, Synthesis and anticancer activity of new hydrazide-hydrazones and their Pd(II) complexes, Lett. Drug Des. Discov. 16 (2018) 522–532, https://doi.org/10.2174/1570180815666180816124102.

[14] E.Q.A. Rasheed, A.Q.A. Rasheed, O.A. Nief, Z.N. Majeed, Synthesis and study properties physical and biological of some dihydrazone derivatives, 6 (2014) 17–25. ISSN 2224- 3224.

[15] P. Rawat, R.N. Singh, Synthesis, spectral and chemical reactivity analysis of 2,4-dinitrophenyl hydrazone having pyrrole moiety, J. Mol. Struct. 1097 (2015) 214–225. doi: 10.1016/j.molstruc.2015.05.020.
[16] B. Evranos-Aksöz, S. Yabanoğlu-Çiftçi, G. Uçar, K. Yelekçi, R. Ertan, Synthesis of some novel hydrazone and 2-pyrazoline derivatives: Monoamine oxidase inhibitory activities and docking studies, Bioorganic Med. Chem. Lett. 24 (2014) 3278–3284, https://doi.org/10.1016/j.bmcl.2014.06.015.
[17] G. Turan-Zitouni, W. Hussein, B.N. Sağlık, A. Tabbi, B. Korkut, Design, synthesis and biological evaluation of novel n-pyridyl-hydrazone derivatives as potential monoamine oxidase (MAO) inhibitors, Molecules 23 (2018) 1–12, https://doi.org/10.3390/molecules23010113.
[18] B.Z. Kurt, I. Gazioglu, L. Basile, F. Sonmez, T. Ginex, M. Kucukislamoglu, S. Guccione, Potential of aryl-urea-benzofuranylthiazoles hybrids as multitasking agents in Alzheimer's disease, Eur. J. Med. Chem. 102 (2015) 80–92, https://doi.org/10.1016/j.ejmech.2015.07.005.
[19] S. Darvesh, I.R. Pottie, K.V. Darvesh, R.S. McDonald, R. Walsh, S. Conrad, A. Penwell, D. Mataija, E. Martin, Differential binding of phenothiazine urea derivatives to wild-type human cholinesterases and butyrylcholinesterase mutants, Bioorganic Med. Chem. 18 (2010) 2232–2244, https://doi.org/10.1016/j.bmc.2010.01.066.
[20] A. Saeed, P.A. Mahesar, S. Zaib, M.S. Khan, A. Matin, M. Shahid, J. Iqbal, Synthesis, cytotoxicity and molecular modelling studies of new phenylcinnamide derivatives as potent inhibitors of cholinesterases, Eur. J. Med. Chem. 78 (2014) 43–53, https://doi.org/10.1016/j.ejmech.2014.03.015.
[21] S. Ke, Z. Li, X. Qian, 1,3,4-Oxadiazole-3(2H)-carboxamide derivatives as potential novel class of monoamine oxidase (MAO) inhibitors: Synthesis, evaluation, and role of urea moiety, Bioorganic Med. Chem. 16 (2008) 7565–7572, https://doi.org/10.1016/j.bmc.2008.07.026.
[22] B.N. Sağlık, B.K. Çavuşoğlu, D. Osmaniye, S. Levent, U.A. Çevik, S. Ilgın, Y. Özkay, Z.A. Kaplancıklı, Y. Öztürk, In vitro and in silico evaluation of new thiazole compounds as monoamine oxidase inhibitors, Bioorg. Chem. 85 (2019) 97–108.
[23] N.Ö. Can, D. Osmaniye, S. Levent, B.N. Sağlık, B. Korkut, Ö. Atlı, Y. Özkay, Z. A. Kaplancıklı, Design, synthesis and biological assessment of new thiazolylhydrazine derivatives as selective and reversible hMAO-A inhibitors, Eur. J. Med. Chem. 144 (2018) 68–81, https://doi.org/10.1016/j.ejmech.2017.12.013.
[24] S. Ilgın, D. Osmaniye, S. Levent, B.N. Sağlık, U. Acar Çevik, B. Kaya Çavuşoğlu, Y. Özkay, Z.A. Kaplancıklı, Design and synthesis of new benzothiazole compounds as selective hMAO-B inhibitors, Molecules 22 (2017) 1–13, https://doi.org/10.3390/molecules22122187.
[25] Ö.D. Can, D. Osmaniye, Ü. Demir Özkay, B.N. Sağlık, S. Levent, S. Ilgın, M. Baysal, Y. Özkay, Z.A. Kaplancıklı, MAO enzymes inhibitory activity of new benzimidazole derivatives including hydrazone and propargyl side chains, Eur. J. Med. Chem. 131 (2017) 92–106, https://doi.org/10.1016/j.ejmech.2017.03.009.
[26] N.Ö. Can, D. Osmaniye, S. Levent, B.N. Sağlık, B. İnci, S. Ilgın, Y. Özkay, Z. A. Kaplancıklı, Synthesis of new hydrazone derivatives for MAO enzymes inhibitory activity, Molecules 22 (8) (2017) 1–19, https://doi.org/10.3390/molecules22081381.
[27] QikProp, version 4.8, Schrödinger, LLC, New York, NY, 2016.
[28] M.M. Morcoss, E.S.M.N. Abdelhafez, R.A. Ibrahem, H.M. Abdel-Rahman, M. Abdel-Aziz, D.A. Abou El-Ella, Design, synthesis, mechanistic studies and in silico ADME predictions of benzimidazole derivatives as novel antifungal agents, Bioorg. Chem. 101 (2020), 103956, https://doi.org/10.1016/j.bioorg.2020.103956.
[29] F. Cheng, W. Li, Y. Zhou, J. Shen, Z. Wu, G. Liu, P.W. Lee, Y. Tang, AdmetSAR: A comprehensive source and free tool for assessment of chemical ADMET properties, J. Chem. Inf. Model. 52 (2012) 3099–3105, https://doi.org/10.1021/ci300367a.
[30] C.A. Lipinski, F. Lombardo, B.W. Dominy, P.J. Feeney, Experimental and computational approaches to estimate solubility and permeability in drug discovery and development settings, Adv. Drug Deliv. Rev. 64 (2012) 4–17, https://doi.org/10.1016/j.addr.2012.09.019.
[31] W.L. Jorgensen, E.M. Duffy, Prediction of drug solubility from structure, Adv. Drug Deliv. Rev. 54 (2002) 355–356. PII: S0169-409X(02)00008-X.
[32] A. Daina, O. Michielin, V. Zoete, SwissADME: A free web tool to evaluate pharmacokinetics, drug-likeness and medicinal chemistry friendliness of small molecules, Sci. Rep. 7 (2017) 1–13, https://doi.org/10.1038/srep42717.
[33] J.D. Dunitz, R. Taylor, Organic fluorine hardly ever accepts hydrogen bonds, Chem. Eur. J. 3 (1997) 89–98.
[34] S.Y. Son, J. Ma, Y. Kondou, M. Yoshimura, E. Yamashita, T. Tsukihara, Structure of human monoamine oxidase A at 2.2-Å resolution: The control of opening the entry for substrates/inhibitors, PNAS 105 (2008) 5739–5744. doi: 10.1073/pnas.0710626105.
[35] Glide, version 7.1, Schrödinger, LLC, New York, NY, 2016.
[36] B.N. Sağlık, S. Ilgın, Y. Özkay, Synthesis of new donepezil analogues and investigation of their effects on cholinesterase enzymes, Eur. J. Med. Chem. 124 (2016) 1026–1040, https://doi.org/10.1016/j.ejmech.2016.10.042.
[37] D. Kwiatek, M. Kubicki, P. Barczyński, S. Lis, Z. Hnatejko, Four new amide derivatives of pyridinecarboxylic acids. Synthesis, structure and spectroscopic characterization, J. Mol. Struct. 1145 (2017) 86–93. doi: 10.1016/j.molstruc.2017.05.080.
[38] P.P. Zhang, Q. Wang, L.J. Min, H. Wu, J. Weng, C. Tan, Y. Zhang, X. Liu, Synthesis, cyrstal structure, fungicidal activity and molecular docking of nicotinic acyl urea derivatives, J. Mol. Struct. 1205 (2020), 127485, https://doi.org/10.1016/j.molstruc.2019.127485.
[39] I.O. Isaac, M. Rashida, S. Rahman, R. Alharthy, A. Asar, A. Hameed, K.M. Khan, J. Iqbal, Acridine-based (thio)semicarbazones and hydrazones: Synthesis, in vitro urease inhibition, molecular docking and in-silico ADME evaluation, Bioorg. Chem. 82 (2018) 6–16, https://doi.org/10.1016/j.bioorg.2018.09.032.
[40] Ü. Demir Özkay, Ö.D. Can, B.N. Sağlık, U. Acar Çevik, S. Levent, Y. Özkay, S. Ilgın, Ö. Atlı, Design, synthesis, and AChE inhibitory activity of new benzothiazole–piperazines, Bioorganic Med. Chem. Lett. 26 (2016) 5387–5394, https://doi.org/10.1016/j.bmcl.2016.10.041.
[41] S. Patel, N. Gheewala, A. Suthar, A. Shah, In-vitro cytotoxicity activity of solanum nigrum extract against Hela cell line and Vero cell line, Int. J. Pharm. Pharm. Sci. 1 (2009) 38–46.